Textile Research Journal
http://trj.sagepub.com/

# An application of queuing theory to modelling of melange yarns. Part II: A method of estimating the fibre migration probabilities and a yarn structure simulation algorithm

Sergei Grishanov, Francois Siewe and Tom Cassidy

*Textile Research Journal* 2011 81: 798 originally published online 26 January 2011
DOI: 10.1177/0040517510391695

The online version of this article can be found at:
http://trj.sagepub.com/content/81/8/798

Published by:
SAGE
http://www.sagepublications.com

**Additional services and information for *Textile Research Journal* can be found at:**

**Email Alerts:** http://trj.sagepub.com/cgi/alerts

**Subscriptions:** http://trj.sagepub.com/subscriptions

**Reprints:** http://www.sagepub.com/journalsReprints.nav

**Permissions:** http://www.sagepub.com/journalsPermissions.nav

**Citations:** http://trj.sagepub.com/content/81/8/798.refs.html

Downloaded from trj.sagepub.com at De Montfort University on September 8, 2011

Original article

Textile Research Journal

Textile Research Journal
81(8) 798–818
© The Author(s) 2010
Reprints and permissions:
sagepub.co.uk/journalsPermissions.nav
DOI: 10.1177/0040517510391695
trj.sagepub.com

SAGE

# An application of queuing theory to modelling of melange yarns. Part II: A method of estimating the fibre migration probabilities and a yarn structure simulation algorithm

**Sergei Grishanov[1], Francois Siewe[2] and Tom Cassidy[3]**

**Abstract**

A queuing model of staple yarn structure was presented in Part I of this work, where the migration behaviours of fibres were simulated by the movement of customers in a Markovian network of queuing systems. Part II of the series proposes (i) a multi-dimensional minimization method for estimating the migration probabilities of fibres based on the analysis of the distribution of number of fibres in yarn cross-sections; (ii) a yarn structure simulation algorithm which uses the migration probabilities of fibres, yarn technical specifications (e.g. linear density and twist) and colour composition to produce a realistic three-dimensional image of a melange yarn. The result is a high quality three-dimensional image of a melange yarn showing its fibrous structure as well as the formation of hairiness. Due to the generic nature of the model and the simulation algorithm, this approach can be applied to a wide range of yarns including ring-spun or open-end spun yarns of solid shade or produced from melange blends. Further improvements to the proposed model are discussed including the application of inhomogeneous Poisson process and the analysis of energy relationships which govern the migration behaviour of fibres.

**Keywords**

Melange yarn, fibre migration, migration probability, queuing system, yarn image

## Introduction

The generation of realistic three-dimensional images of yarns in the context of computer-aided design of textile materials requires detailed knowledge of yarn structure which ultimately should include information on the spatial location of every fibre in the yarn body. More specifically, the fibre packing density distribution over the melange yarn cross-section (and in particular in the area which is close to the yarn surface) determines the conditions of light reflection and scattering and thus affects the yarn colour. In this respect, an ability to predict the fibre packing density distribution is important for the prediction of the colour of melange yarns and fabrics.

Part I of this series[1] suggested a new model which can provide this information subject to the knowledge of yarn technical specifications (e.g. linear density and twist) and some additional parameters such as migration probabilities describing the fibre migration in the yarn. It has been shown in Part I that accurate estimation of migration probabilities presents a difficult task both in terms of the experimental technique required and the mathematical treatment of the problem. An attempt to use this model to predict the packing density distribution and the average number of fibres in the yarn cross-section[1] showed a poor agreement

[1]TEAM Research Group, De Montfort University, UK.
[2]Software Technology Research Laboratory, De Montfort University, UK.
[3]School of Design, Leeds University, UK.

**Corresponding author:**
Sergei Grishanov, TEAM Research Group, De Montfort University, The Gateway, Leicester, LE1 9BH, UK
Email: gsa@dmu.ac.uk.

Downloaded from trj.sagepub.com at De Montfort University on September 8, 2011

with the experimental data. One of the reasons identified was that the experimentally estimated migration probabilities were not unconditional probabilities as required by the model.

The problem of fibre migration in yarns received a lot of attention in the 1960s as at that time it was recognized that it has a significant influence on the appearance and performance characteristics of yarns and thus required a detailed investigation. Hearle and his co-workers[2–7] and also Riding[8] and Treloar[9] made significant contributions to the development of the understanding of fibre migration. In a series of papers[2,5–7] a mechanism of migration was considered using a simplified model where:

1. A yarn was considered as made from seven continuous filaments which were represented by seven single yarns continuously supplied under a controlled tension and twisted together into a rope-like structure.[2]
2. The migrating filaments were arranged into a single layer at the nip of the front rollers[2] whereas in real yarns, fibres passing through the nip of the front rollers occupy several intermeshing layers. The experimental modelling of two- and three-layered arrangements of filaments showed a more complex picture of filament migration but this has not been fully analysed.[5–7]
3. The migrating filaments were assumed to be initially straight without any crimp.
4. Friction forces between the filaments were ignored.
5. Due to the small number of filaments considered, the maximum complexity of the yarn cross-section which could be achieved was a simple structure with two,[2] or three[7] fully occupied ring zones. Thus complex relationships affecting multiple inter-zone migrations were not considered.
6. In the analysis of fibre migration the yarn cross-section was divided into ring zones of equal area.[3] This inevitably leads to a single central zone accommodating many fibres which would be contained within several ring zones of equal width.[3] This method of division may generate a narrow outermost zone the width of which could be less than the diameter of a single fibre. This approach does not provide means for modelling the migration of individual fibres.
7. The packing density of fibres in the yarn was assumed to be constant throughout the yarn[3] which is not the case in real staple-fibre yarns.

Due to the limitations of this model the conclusion was made that it is the difference in tension between the fibres on the yarn periphery and the yarn centre that is the main factor affecting the migration. However, it was noted that the actual mechanism of migration is much more complex and may be considered as a combination of two tendencies: one explained by the difference in tension and the second explained by geometrical principles.[4]

When modelling yarn structure based on fibre migration in staple fibre yarns, it is necessary to take into account a number of factors, many of which have a significant degree of randomness.

The cross-section of a staple fibre yarn may be made of tens or even hundreds of individual fibres. For example, a fine 6 tex cotton yarn produced from 0.15 tex fibres would have on average of 40 fibres in a cross-section whereas a 100 tex woollen yarn may have 250 fibres in the cross-section. In order to be able to model the spatial position of each individual fibre, it is necessary to use a model which is capable of handling this. For this reason a model based on ring zones of equal width and circular virtual locations[1,10,11] was adopted for this investigation. Recently, an improved version of this model has been reported[12] where energy analysis of migrating fibre has been done and virtual locations (VL) had elliptical shapes depending on the yarn twist level. However, the introduction of this model would require the relationship between the twist and actual shape of VL to be investigated in detail. The analysis of energy did not compare the effects of its different components but rather concentrated on the dominance of tension as the main cause for the migration, thus providing a link between energy and migration. The computer generated images of yarn cross-sections showed too densely populated cross-sections in comparison with those of real yarns.

It was assumed in the present model that the migration takes place within the twist triangle. The total number of fibres currently present in the twist triangle can be divided into three groups where each group, on average, would consist of a third of the total number of fibres. The exact number of the fibres in each group may deviate from this number due to the random position of fibres along the yarn axis, the variation of the fibre length, and the variation of the length of the twist triangle. Figure 1 illustrates a simple case of 15 fibres arranged into a single layer where fibres are randomly assigned to one of three groups; there are four fibres in Group 1, five in Group 2, and six in Group 3. Fibres in Group 1 have their leading ends free to migrate because they have not been fixed in the yarn yet. In a similar manner, fibres in Group 2 would have their trailing ends free to migrate because they have left the nip of the front rollers but are not fixed in the yarn structure. The fibres in Group 3 would have their leading ends, which passed the point of yarn formation, fixed in the yarn structure whereas their trailing ends are still in the drafting zone. Portions of the fibres' length between the nip of the front roller and the point of

Downloaded from trj.sagepub.com at De Montfort University on September 8, 2011

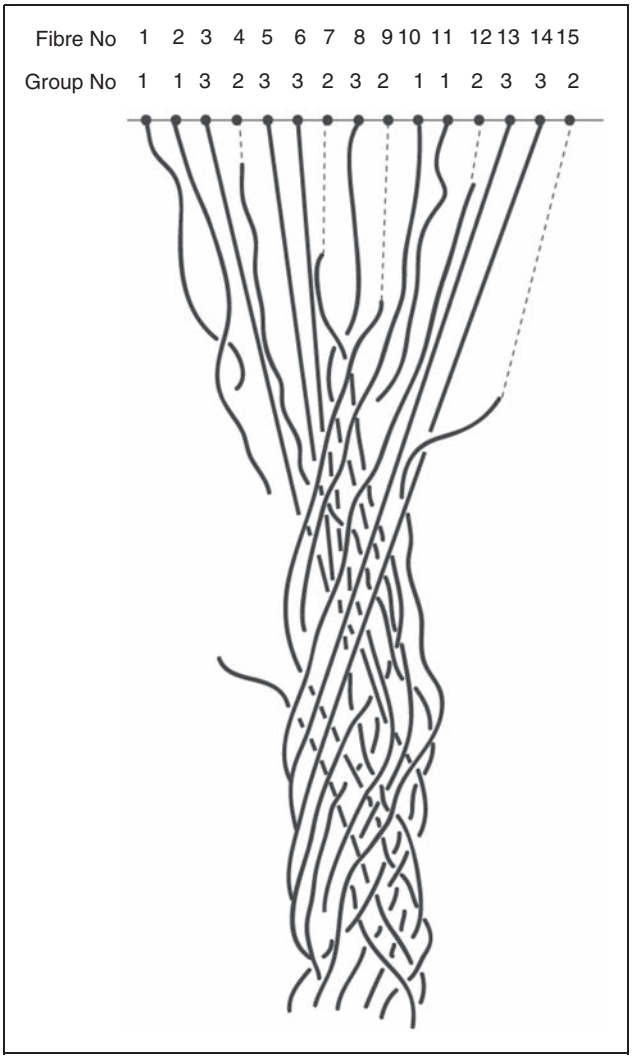



**Figure 1.** A schematic representation of yarn formation.

yarn formation would be under tension depending on their position in the nip and in the yarn structure being formed. Their migration would be governed by the difference in tension in combination with other factors such as friction.

Similar to the movement of floating fibres in the drafting zone, it would not be possible to identify precisely whether or not the trailing and the leading ends of fibres would migrate, at which point, and in which direction due to a number of random factors. These factors include friction between the fibres, random spatial shape of the fibres, the distribution of fibre diameters, and the current distribution of fibres in the yarn cross-section being formed. In the same way, the migration of the fibres in Group 3 is affected by the same factors as above and the variation of tensile force applied in the spinning process.

Theoretically, there is a large number of ways in which fibres coming out of the nip of the front rollers can be arranged into a yarn. This number can be estimated as $A_n^p = C_n^p p! = \frac{n!}{(n-p)!}$[13] where $n$ is the number of virtual locations and $p$ is the number of fibres, $n \geq p$. Using the approach suggested in Part I[1], from the example in Figure 1 it can be seen that the minimum number of virtual locations which could accommodate $p = 15$ fibres would be $n = 19$ in a three-zone yarn. In this case the number of possible fibre arrangements is approximately $5 \times 10^{15}$. Obviously, it would not be possible to realise many of these arrangements due to the restrictions imposed by fibre and yarn mechanics. This number, however, illustrates that there is a need for a different approach to modelling the fibre migration rather than that based on simplified mechanics of fibre assembly.

A universal characteristic, which can be suggested for the characterization of the migration of each individual fibre in a complex situation where many fibres interact with each other, is a migration probability.[1,11] The migration process can be considered as a purely random process where the migration of each individual fibre depends on a large number of random factors. Alternatively, an attempt can be made to relate the migration probability to the energy relationships in the fibre assembly. The latter approach, however, would require significant simplifications to be introduced in order to make the analysis at all possible. In any case the distribution of the migration probability must be such that it provides the experimentally known fibre distribution over the yarn cross-section.

This paper continues the investigation of yarn structure reported in earlier publications[1,11] and presents a much better method for estimating the migration probabilities which shows a very good agreement with the experiments. This information is then used in a new software tool for generating realistic three-dimensional images of melange yarns.

The sections that follow briefly discuss the queuing model used in Part I[1] for the description of the migration behaviour of fibres in the staple fibre yarn; introduce a new mathematical model of fibre migration and a new method of estimating the migration probabilities; and then present an algorithm for computer modelling and visualization of realistic three-dimensional images of staple fibre yarns together with examples of melange yarn images.

## Overview of the queuing model of yarn structure

The queuing model of yarn structure, presented in Part I, describes the migration behaviour of fibres in a yarn body by analogy to the behaviours of customers in a network of Markovian queuing systems where customers move between queuing systems of the network

Downloaded from trj.sagepub.com at De Montfort University on September 8, 2011

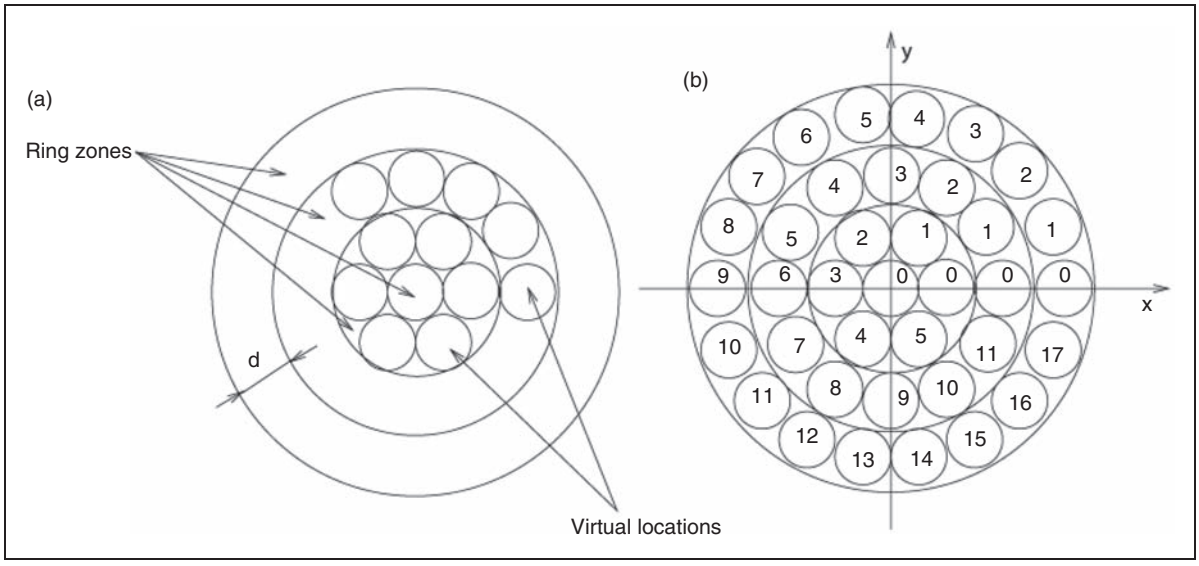



**Figure 2.** A yarn cross-section model according to Part I.[1]: (a) Ring zones and Virtual Locations, (b) Numvering of virtual Locations.

to get served. The model assumes that the structure of a yarn cross-section is a set of $K$ concentric circular ring zones around the yarn centre, as depicted in Figure 2.[1] The ring zones are assumed to have identical width $d = \bar{d}_f + \sigma_f$ where $\bar{d}_f$ and $\sigma_f$ are the average and the standard deviation of the fibres' diameters, respectively. Each ring zone is divided into a fixed number of virtual locations (VLs) represented as circles of the same diameter, $d$, as shown in Figure 2a.

The ring zones are numbered from zero to $K-1$ starting from the yarn centre and progressing towards the yarn surface. The ring zone 0 is situated at the yarn centre and consists of exactly one VL. A ring zone $i$, $1 \le i < K$, contains $\lfloor 2\pi i \rfloor$ (i.e. the greatest integer less than or equal to $2\pi i$) VLs. In this way the ring zone 1 contains six VLs, the ring zone 2 contains 12, the ring zone 3 contains 18 and so on as depicted in Figure 2b. Let $E_i$ denote the set of all virtual locations in the ring zone $i$; $E_0 = \{0\}$ and $E_i = \{x \in N | 0 \le x < \lfloor 2\pi i \rfloor\}$, for $i > 0$. The number of virtual locations in zone $i$ is then $z_i = |E_i|$. The virtual locations of each zone $i$ are numbered counter-clockwise from 0 to $z_i - 1$ and the virtual location 0 is centred on the $x$-axis as illustrated in Figure 2b. The virtual location, $r$, of the ring zone, $i$, is referred to by the pair $(i, r)$.

In the model, each virtual location is represented by a queuing system and each fibre is modelled by a customer. The migration of a fibre from one virtual location to a neighbouring virtual location is associated with the movement of a customer from one queuing system to another. It is supposed that the distances between fibre leading-ends in a VL $(i, r)$ are exponentially distributed with parameter $\lambda^0_{ir}$. Thus, a new fibre arrives to the VL $(i, r)$ according to a homogeneous Poisson process with a constant rate $\lambda^0_{ir}$. After remaining in the VL $(i, r)$ for a migration distance, which is assumed exponentially distributed, the fibre either terminates with probability, $p^0_{ir}$, or migrates into a VL $(j, s)$, with probability $p_{ir;js}$. It is assumed that a fibre can only take an elementary migration action (see Definition 3.2 in Part I) in any single migration step. Therefore the probability, $p_{ir;js}$, for a fibre to migrate in one step from the VL $(i, r)$ to the VL $(j, s)$ is 0 if the VL $(j, s)$ is not in the closest neighbourhood $I_{ir}$ of the VL $(i, r)$ as has been discussed in Part I.[1] On the basis of this the normalization condition is given by:

$$\left(\sum_{(j,s)\in I_{ir}} p_{ir;js}\right) + p^0_{ir} = 1, \quad \text{for} \quad 0 \le i < K \text{ and } 0 \le r < z_i, \tag{1}$$

where $z_i = |E_i|$.

The total arrival rate of fibres in the VL $(i, r)$ is given by:

$$\lambda_{ir} = \lambda^0_{ir} + \sum_{j=0}^{K-1} \sum_{s=0}^{z_i - 1} p_{js;ir} \lambda_{js}, \quad \text{for} \quad 0 \le i < K \text{ and } 0 \le r < z_i. \tag{2}$$

The system state is characterized by a vector $(n_{00}, n_{10}, \ldots, n_{K-1, \lfloor 2\pi(K-1) \rfloor - 1})$ such that each component $n_{ir}$ is the number of fibres in the queuing system modelling the VL $(i, r)$, $0 \le i < K$ and $0 \le r < z_i$. A method for estimating the fibre migration and termination probabilities is presented in the following section.

The probability $p_{ij}$ of a fibre to migrate from ring zone $i$ to ring zone $j$ is obtained from the probability distribution of fibre migration between virtual locations, $p_{ir;js}$, presented above by taking the normalized

Downloaded from trj.sagepub.com at De Montfort University on September 8, 2011

sum of the probabilities for migrating from a VL in the ring zone $i$ to a VL in the ring zone $j$, viz

$$\left.\begin{array}{l} p_{01} = \sum_{r=0}^{5} p_{00;1r}, \text{ if } i = 0; \\ p_{ij} = \frac{1}{z_i} \sum_{r=0}^{z_i-1} \sum_{(j,s)\in I_{ir}} p_{ir;js}, \text{ if } i > 0; \\ z_i = |E_i|; \end{array}\right\}. \quad (3)$$

where $I_{ir}$ is the closest neighbourhood of the VL $(i, r)$. Therefore, $p_{ij}=0$ when $|j-i|>1$ as an elementary migration can only happen within a ring zone or between two adjacent ring zones (see Definition 3.2 in Part I).

Similarly, the probability $p_{it}$ of a fibre terminating in a ring zone $i$ is

$$\left.\begin{array}{l} p_{0t} = p_{00}^{0}, \text{ if } i = 0; \\ p_{it} = \frac{1}{z_i} \sum_{r=0}^{z_i-1} p_{ir}^{0}, \text{ if } i > 0; \\ z_i = |E_i|; \end{array}\right\}. \quad (4)$$

The probabilities of fibre migration between the ring zones and fibre termination defined in Equations 3 and 4 will be used in the next section for modelling the process of migration.

## Modelling the fibre density distribution over the yarn cross-section

A yarn made of staple fibres is a product of an ever changing but, if averaged over a long length, stable linear density. Assuming that the fibres themselves have a constant linear density then the variation in the yarn linear density should result from the variation in the number of fibres in the yarn cross-sections which in turn is caused by new fibres coming and some fibres terminating. Many investigations confirmed that despite the fibre migration between the ring zones being a random process the distribution of the number of fibres in the ring zones has a typical shape which depends on the linear density and twist factor of the yarn.[10,14–17] Thus, it is reasonable to assume that the fibre migration happens in a specific way which, together with a flow of fibres coming and terminating, provides a dynamic equilibrium to the yarn structure.

This paper considers two approaches to modelling the fibre migration. One is based on an attempt to link the migration probabilities with the energy relationships governing the movement of fibres in the yarn body. Indeed, at any given point at the yarn cross-section, a fibre has a random spatial shape which is the result of its initial random shape and the actions of the external forces acting on fibres in spinning. In this respect, it is reasonable to assume that the deviation of fibre shape from its natural configuration can be characterized by the potential energy of elastic deformation. The fibre thus is trying to change its shape by reducing the level of potential energy stored and all other surrounding fibres do so as well. The combination of these two factors, i.e. action of external forces and natural tendency of the fibre to take the position corresponding to the minimum internal energy, causes the fibres to move from one VL to another with some probability. In this way, fibre migration can be considered either during the yarn formation or immediately after the yarn has been spun. A discourse on this energy-based approach is presented in the 'Discussion of influencing factors' section.

However, it would be extremely difficult to estimate the magnitude of all forces acting on every fibre at every point in the yarn and to predict the dynamics of fibre migration using this information. For this reason, the second and simpler approach applies the queuing theory to modelling the migration pattern of the fibre in question between the VLs. This leads to equations that express the change in the number of fibres in the yarn cross-sections and ring zones through the migration probabilities. The whole process is assumed to be memoryless (this is one of the requirements for applying queuing theory), i.e. that the movement of fibres from one VL to another between two consecutive cross-sections $L$ and $L+1$ depends only on the conditions at the cross-section $L$ but not on any previous movements.

Considering two consecutive cross-sections $L$ and $L+1$, these assumptions are made:

1. The number of fibres migrating from zone $i$ of cross-section $L$ to zone $i+1$ or $i-1$, if they exist, in cross-section $L+1$ is proportional to the number of fibres in zone $i$ in the cross-section $L$ and the relative number of non-occupied virtual locations in zone $i+1$ or $i-1$ in the cross-section $L$, respectively.
2. The number of new fibres coming into zone $i$ in cross-section $L+1$ is proportional to the number of non-occupied virtual locations available in this zone in cross-section $L$.
3. The number of fibres terminating in zone $i$ of cross-section $L$ is proportional to the number of fibres in zone $i$ of cross-section $L$.

Based on these assumptions, the equation which links the number of fibres in the central zone $i=0$ of the cross-sections $L$ and $L+1$ can be written as follows:

$$\begin{aligned} n_0^{L+1} = n_0^L + p_{10} n_1^L \frac{z0 - n_0^L}{z_0} + p_{0n}\left(z0 - n_0^L\right) \\ - p_{0t} n_0^L - p_{01} n_0^L \frac{z_1 - n_1^L}{z_1}, \end{aligned} \quad (5)$$

Downloaded from trj.sagepub.com at De Montfort University on September 8, 2011

where $n_i^{L+1}$ and $n_i^L$ are the number of fibres in zone $i$ in the cross-sections $L$ and $L+1$, respectively;

$z_i = |E_i|$ is the number of virtual locations in the zone $i$;

$p_{10}$ is the probability for a fibre to migrate from zone 1 to zone 0;

$p_{0n}$ is the probability for a new fibre to come into zone 0;

$p_{0t}$ is the probability for a fibre to terminate in zone 0;

$p_{01}$ is the probability for a fibre to migrate from zone 0 to zone 1.

The second, third, fourth, and the last term in Equation 5 give, respectively, the number of fibres migrating from zone 1 down to zone 0, the number of new fibres coming into zone 0, the number of fibres terminating in zone 0, and the number of fibres leaving zone 0 to zone 1.

The number of fibres in a middle zone $i$, $0<i<K-1$, is affected by the fibres migrating from this zone towards the yarn centre (zone $i-1$) and towards the outer zone $i+1$, by the fibres migrating into this zone from both zone $i-1$ and zone $i+1$, by new coming fibres, and by fibres terminating in this zone. Therefore the equation in this case is as follows:

$$\begin{aligned} n_i^{L+1} = {} & n_i^L + p_{i-1,i}\, n_{i-1}^L \frac{z_i - n_i^L}{z_i} + p_{i+1,i}\, n_{i+1}^L \frac{z_i - n_i^L}{z_i} \\ & + p_{in}\left(z_i - n_i^L\right) - p_{i,i+1} n_i^L \frac{z_{i+1} - n_{i+1}^L}{z_{i+1}} \\ & - p_{i,i-1} n_i^L \frac{z_{i-1} - n_{i-1}^L}{z_{i-1}} - p_{it} n_i^L . \end{aligned} \tag{6}$$

Finally, the number of fibres in the outermost zone can be described by the equation as follows:

$$\begin{aligned} n_{K-1}^{L+1} = {} & n_{K-1}^L + p_{K-2,K-1} n_{K-2}^L \frac{z_{K-1} - n_{K-1}^L}{z_{K-1}} \\ & + p_{K-1} n(z_{K-1} - n_{K-1}^L) - p_{K-1,K-2} n_{K-1}^L \\ & \times \frac{z_{K-2} - n_{K-2}^L}{z_{K-2}} - p_{K-1t} n_{K-1}^L . \end{aligned} \tag{7}$$

For a yarn with $K$ zones there are $K$ linear equations but $4K-2$ unknown probabilities $p_{ij}$, $p_{it}$, and $p_{in}$. Thus, it is not possible to find a solution of these linear equations by the usual method. However, this paper suggests a way for estimating these probabilities using a multi-dimensional minimization method.

## A method for estimating the fibre migration probabilities

It can be shown that, subject to some additional conditions, an iterative application of equations 5–7 converges to steady-state values of the number of fibres in the ring zones which depend on the values of probabilities $p_{ij}$, $p_{it}$, and $p_{in}$. Figure 3 illustrates a simple case of four ring zones where the values of probabilities were fixed as follows: $p_{10}=0.1$; $p_{21}=0.3$; $p_{32}=0.5$; $p_{01}=0.5$; $p_{12}=0.4$; $p_{23}=0.3$; $p_{0n}=0.2$; $p_{1n}=0.1$; $p_{2n}=0.1$; $p_{3n}=0.1$; $p_{0t}=0.1$; $p_{1t}=0.2$; $p_{2t}=0.1$; $p_{3t}=0.1$.

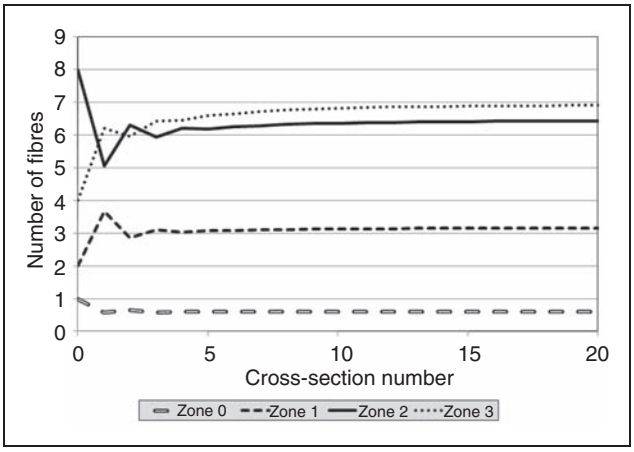



**Figure 3.** Convergence to steady-state values of the number of fibres in the ring zones 0, 1, 2, and 3.

Thus, it is necessary to find the values of these unknown probabilities $p_{ij}$, $p_{it}$, and $p_{in}$ that provide the minimum difference between the experimentally known average number of fibres in the ring zones $(n_0^e, n_1^e, \ldots n_{K-1}^e)$ and the steady-state number of fibres $(n_0^*, n_1^*, \ldots n_{K-1}^*)$ obtained from the iterations. This is essentially a multi-dimensional minimization problem.

The minimization algorithm consists of two nested iterations (see Figure 4). The inner iteration uses equations 5–7 in order to calculate the steady-state number of fibres $(n_0^*, n_1^*, \ldots n_{K-1}^*)$ for a given set of probabilities $p_{ij}$, $p_{it}$, and $p_{in}$. The convergence to a steady-state is checked against a specified small threshold value $\delta$. The set $(n_0^*, n_1^*, \ldots n_{K-1}^*)$ is then used to calculate the value of the objective function (8). The outer iteration employs Powell's method[18] in order to find a set of probabilities such that objective function $F$ takes its minimum value within a specified accuracy $\varepsilon$.

The objective function for this minimization problem can be written as follows:

$$\begin{aligned} F(p_{ij}, p_{it}, p_{in}) = {} & \sum_{m=0}^{K-1} \{n_m^e - n_m^*(p_{ij}, p_{it}, p_{in})\}^2 \\ & + G(n_0^*, n_1^*, \ldots, n_{K-1}^*) + H(p_{ij}, p_{it}, p_{in}) \to \min , \end{aligned} \tag{8}$$

where $G(n_0^*, n_1^*, \ldots, n_{K-1}^*)$ and $H(p_{ij}, p_{it}, p_{in})$ are penalty functions. Note that $n_i^*$ are functions of probabilities $p_{ij}$, $p_{it}$, and $p_{in}$.

Downloaded from trj.sagepub.com at De Montfort University on September 8, 2011

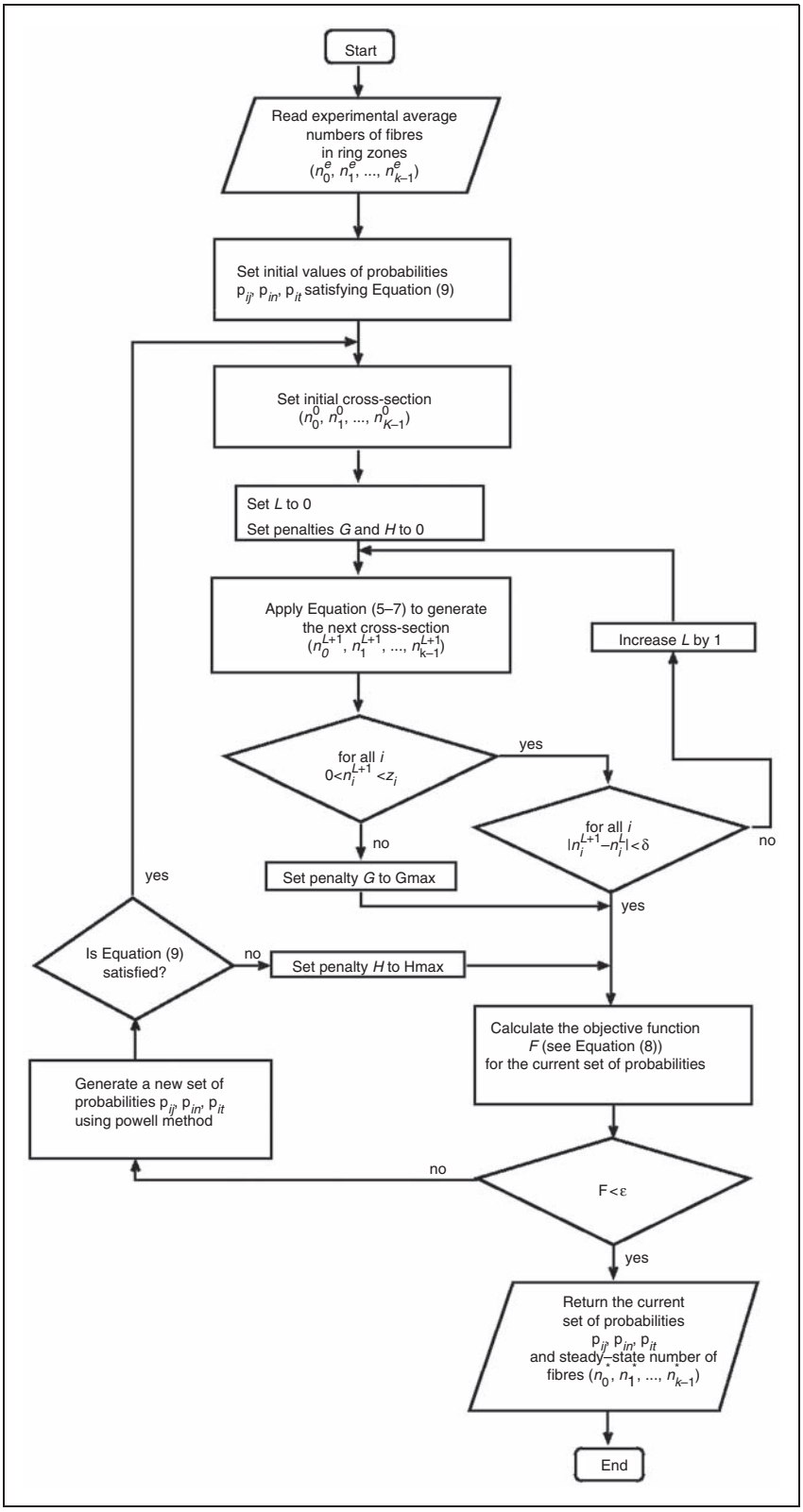



**Figure 4.** A flow diagram for the algorithm calculating probabilities $p_{ij}$, $p_{it}$, and $p_{in}$.

Downloaded from trj.sagepub.com at De Montfort University on September 8, 2011

The penalty function $G$ returns a zero value if all of the $n_i^*$ are within admissible limits, i.e. if they are all positive and do not exceed the number of virtual locations in the respective zones. However, some of these $n_i^*$ may be negative or exceed the number of virtual locations in the zone $i$. In this case, the inner iteration is terminated and the penalty function $G$ returns a large penalty value, $G_{max}$.

The penalty function $H$ returns a zero value if all probabilities $p_{ij}$, $p_{it}$, and $p_{in}$ are between 0 and 1 and satisfy the normalization condition as follows:

$$\left.\begin{array}{l} p_{00}+p_{01}+p_{0t}=1; \\ \sum\limits_{j=i-1}^{i+1} p_{ij}+p_{it}=1, \text{for } 0<i<K-1; \\ p_{K-1,K-1}+p_{K-1,K-2}+p_{K-1t}=1. \end{array}\right\}. \quad (9)$$

Otherwise the penalty function $H$ returns a large penalty value, $H_{max}$.

The evaluation of this algorithm against experimentally obtained average number of fibres in the ring zones is discussed in the Results section; the yarn samples used for this evaluation are specified in the experimental section in Tables 1, 3 and 4.

## Yarn structure simulation algorithm

The models discussed in the above sections provide necessary information for the three-dimensional simulation of a detailed yarn structure. This section introduces a yarn simulation algorithm where a length of yarn is created as a series of cross-sections as depicted in Figure 5. Each cross-section represents a migration point, i.e. a position along the yarn axis where a fibre may change the virtual location. The distances between the cross-sections are equal to the migration distances according to Definition 3.3[1] and are assumed to be exponentially distributed. This is justified by the underlying network of $M/M/1$ queues model of staple fibre yarn presented in Part I.[1] For the same reason, the distances between the leading-ends of fibres within a yarn, which correspond to the inter-arrival times of new fibres in the yarn, are assumed to follow an exponential distribution. However, in both cases other distributions, such as a deterministic distribution and a general distribution, might be considered.

It is assumed that the following characteristics of a melange yarn are known:

- the linear density and the twist level;
- the number of colours and the percentage of fibres of each colour in the melange yarn;
- the average fibre length and standard deviation;
- the average fibre diameter and standard deviation;
- the occupancy probabilities of ring zones; these determine the distribution of number of fibres in the ring zones.

A fibre is represented by a data structure that stores the fibre's characteristics listed above and its starting $z$-position along the yarn axis. It is assumed that fibre lengths and fibre diameters follow a normal distribution. Fibres are randomly assigned colours according to the colour composition (or colour percentages) of the melange yarn.

First, the migration probabilities are calculated using the algorithm described in Figure 4 in 'A method for estimating the fibre migration probabilities' section, with the input being the average number of fibres in ring zones obtained from the occupancy probabilities.

Then the virtual path of a fibre is constructed iteratively as a three-dimensional cubic spline that ensures that the fibre passes through the specified set of points in three-dimensions and minimizes the fibre's potential energy of deformation for this set (please see Appendix 1). Spline approximation also ensures that the fibre does not break but keeps a smooth shape as it moves in the yarn body. Initially, the fibre is assigned a virtual location $(i, r)$ in the yarn cross-section it starts from, based on the occupancy probabilities of the ring zones of the yarn cross-sections. The migration probabilities are used to determine the neighbouring VL into which the fibre can migrate in the next cross-section. Then the angle of twist is calculated and the path of the fibre to that VL is approximated as a three-dimensional cubic spline. The length of the spline curve corresponds to the length of the portion of the fibre used up to the current cross-section. Then, the fibre migrates through further cross-sections in the same manner until its total length is used or the yarn simulation terminates.

The algorithm used to construct a yarn can be summarized as follows:

**Algorithm** MelangeYarn Structure
**Input:**

- yarn linear density
- yarn twist level
- number of colours and percentages of fibres of each colour in the composition
- occupancy probabilities of ring zones
- average fibre length and standard deviation
- average fibre diameter and standard deviation

**Method:**

Step 1. Calculate the migration probabilities using the algorithm described in the previous section, 'A method for estimating the fibre migration probabilities'.
Step 2. Assign each fibre

Downloaded from trj.sagepub.com at De Montfort University on September 8, 2011

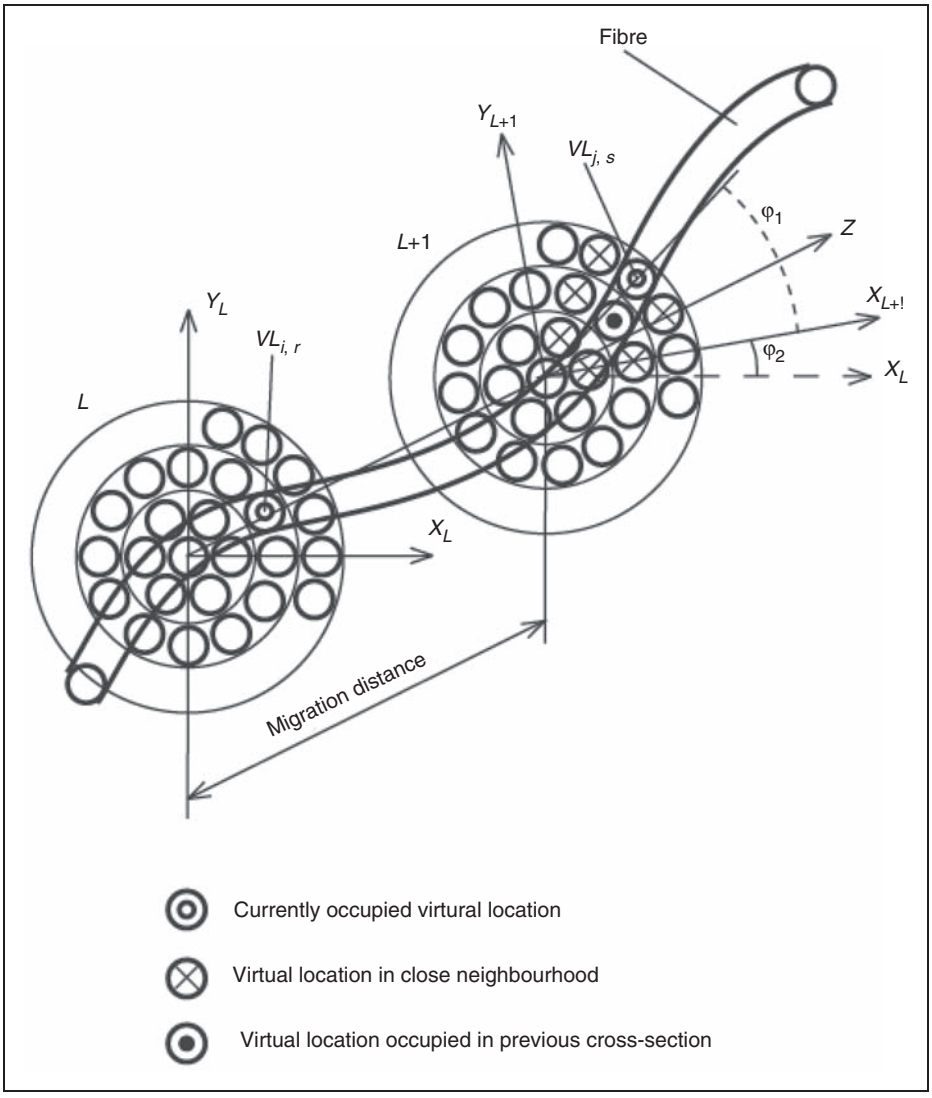



**Figure 5.** Yarn structure represented by a series of cross-sections.

- a random starting point on the yarn axis (the distances between these points are exponentially distributed);
- a random colour, based on the colour percentages of the melange yarn;
- a random length and a random diameter using a normal distribution.

Step 3. Create the first cross-section of the yarn.
Step 4. Assign each fibre, starting at that cross-section, a virtual location based on the occupancy probabilities of the ring zones;
Step 5. Create a new cross-section (distances between the cross-sections are exponentially distributed).
Step 6. Migrate fibres from the previous cross-section into the new cross-section as follows:

For each fibre in the previous cross-section

Step 6.1. Determine the VL of the new cross-section the fibre is migrating into using the migration probabilities;
Step 6.2. Calculate the angle of twist between the origin VL and the destination VL, and approximate the path of the fibre from origin VL to the destination VL by a three-dimensional cubic spline;
Step 6.3. If the fibre is long enough to reach the destination VL in the new cross-section as it follows its spline curve then migrate the fibre into that VL;
Step 6.4. If that fibre is not long enough to reach the new cross-section, it terminates somewhere before the new cross-section as it follows its spline curve. In this case, the destination VL will still be available to other fibres.
Step 7. Assign each new fibre that starts at the new cross-section or between it and the previous one a VL

Downloaded from trj.sagepub.com at De Montfort University on September 8, 2011

in the new cross-section, according to the occupancy probabilities of the ring zones.
Step 8. If more yarn length is needed then go to Step 5.

**End**

This algorithm was implemented as a multi-document interface application for Windows and produced realistic three-dimensional images of melange yarns as shown in the Results section.

## Experiments

The experimental investigation concentrated on the study of fibre packing density in yarn cross-sections. For this, data from three different sources was gathered. First, this was information on the number of fibres in the ring zones of eight yarns (yarn sample series Y) reported by Grishanov et al.,[10] see Table 1. Then, thirty independent cross-sections randomly positioned at least 2 m apart from each other were taken from each of eight melange yarns different in blend composition (yarn sample series M). These 55 tex/340 twist/m yarns were spun using the same spinning equipment and from the same acrylic fibre as those reported in Part I.[1] Fibre length distribution for red, green, and blue fibres was measured using a WIRA Fibre Diagram Machine; the distribution of fibre diameter was measured using a LaserScan. Fibre length and diameter characteristics for the acrylic fibres are given in Table 2. Also, the yarn samples used in Part I[1] (yarn sample series S) were re-examined in order to obtain more information on the fibre packing density distribution.

The experimental data on the fibre distribution in the ring zones of all yarns was processed using the method of multi-dimensional minimization discussed in the 'A method for estimating the fibre migration probabilities' section above. The results showed a high correlation between the experimental and predicted distributions (see Tables 1, 3, and 4).

## Results

This section describes the results of the application of algorithms, presented in the sections above, to the experimental data on fibre distribution in the yarn cross-sections. The simulated melange yarn images produced by the yarn simulation algorithm are presented as well.

### *Predicting the fibre density distribution*

The experimental data on the number of fibres in the yarn ring zones was supplied to the algorithm which calculates the unknown migration probabilities $p_{ij}$, $p_{it}$, and $p_{in}$ and evaluates the number of fibres in the yarn ring zones $(n_0^*, n_1^*, \ldots, n_{K-1}^*)$ at the steady-state which is based on these probabilities. The total number of fibres in the yarn cross-section was estimated as

$$N_T^* = \sum_{i=0}^{K-1} n_i^*. \tag{10}$$

**Table 2.** Characteristics of acrylic fibre

| | Fibre length, mm | | Fibre diameter, micron | |
|---|---|---|---|---|
| Fibre type | Average | Standard deviation | Average | Standard deviation |
| Red | 98.8 | 38.48 | 23.2 | 3.71 |
| Green | 95.3 | 38.85 | 23.5 | 2.96 |
| Blue | 97.7 | 37.25 | 23.8 | 3.17 |

**Table 1.** Experimental and predicted average number of fibres for sample series Y

| Sample | Yarn linear density, tex[a] | Yarn twist level, tpm[a] | Total number of fibres | | Relative error, % | Correlation coefficient |
|---|---|---|---|---|---|---|
| | | | Experimental[b] | Predicted | | |
| Y1 | 70 | 230 | 123.2 | 112.8 | 8.45 | 0.959 |
| Y2 | 150 | 140 | 434.3 | 442.0 | 1.76 | 0.997 |
| Y3 | 70 | 340 | 156.3 | 159.1 | 1.79 | 0.995 |
| Y4 | 150 | 203 | 427.2 | 430.1 | 0.68 | 0.985 |
| Y5 | 52 | 340 | 124.3 | 112.7 | 9.37 | 0.955 |
| Y6 | 167 | 155 | 478.1 | 491.6 | 2.83 | 0.972 |
| Y7 | 110 | 165 | 286.5 | 289.3 | 0.99 | 0.994 |
| Y8 | 110 | 265 | 267.5 | 265.0 | 0.92 | 0.980 |

[a]Yarn linear density and twist level are according to Grishanov et al.,[10] Table 1.[b]Experimental number of fibres is according to Grishanov et al.,[10] Figure 2a, 2b, and 2c.

Downloaded from trj.sagepub.com at De Montfort University on September 8, 2011

It can be seen that the predicted number of fibres in the ring zones closely follows the experimental distributions. Indeed, Table 1 shows a small average error of 3.35% in predicting the total average number of fibres in the cross-sections; the correlation between the experimental and predicted distributions was very high ranging from 0.955 (sample Y5) to 0.997 (sample Y2). No correlation was found between the technical parameters of yarns, such as linear density, twist level, and twist factor, and relative errors. This confirms that the errors in predicting the number of fibres are of a random nature and do not depend on yarn parameters. Figures 6a–c illustrate the experimental and predicted results for the distribution of the number of fibres obtained for samples Y2, Y4, and Y5.

Table 3 presents a comparison between the experimental and the predicted number of fibres in the melange yarns cross-sections; Figure 7 is an example of fibre distribution for sample M1. This table shows a very good match between the experimental and the predicted distributions characterized by a high correlation between the experimental and predicted values between 0.995 and 0.999 and a small average error of 0.6% in estimating the total number of fibres in a yarn cross-section.

This method was also applied to four yarn samples considered in Part I;[1] the results are presented in Table 4. It can be seen that the new method gives much better results than those obtained in Part I.[1]

Overall, it was noticed that in the majority of cases there was a small difference between the experimental and predicted number of fibres in the outermost zones for all yarns. This can be attributed to a cut-off effect due to which only a limited number of ring zones has been considered for each sample which constitutes the main body of the yarn containing 95% of the average number of fibres in the cross-section. In fact the yarn has an opened structure which may extend over many ring zones so that there may be a small number of fibres

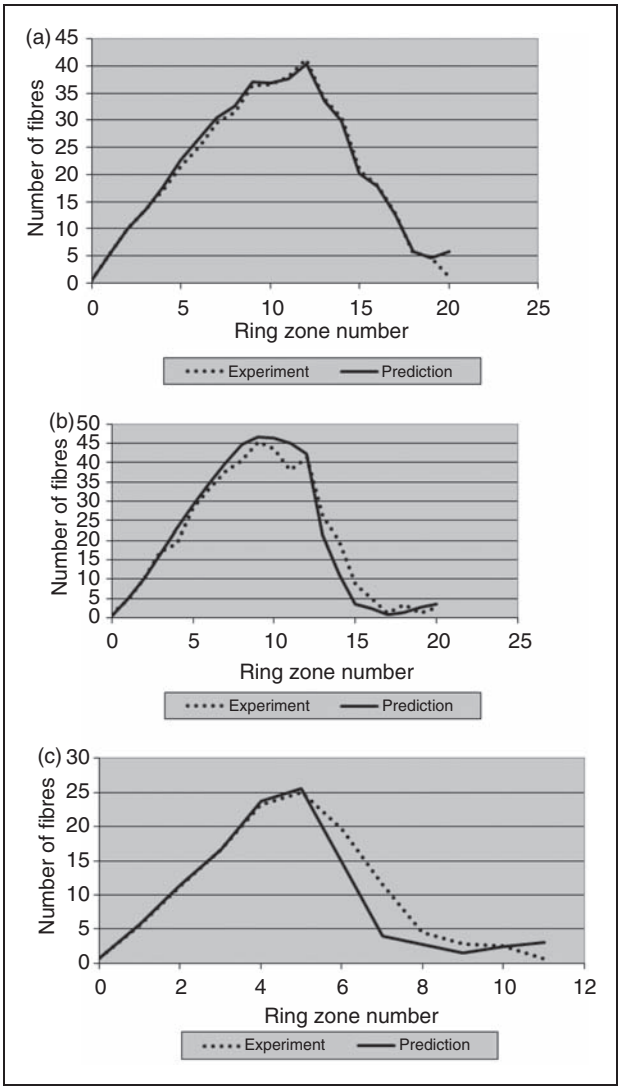



**Figure 6.** Predicted and experimental distributions of the number of fibres in the yarn zones; (a) sample Y2, (b) sample Y4, (c) sample Y5.

**Table 3.** Experimental and predicted average number of fibres for samples series M

| Sample | Composition, % | | | Total number of fibres | | Relative error, % | Correlation coefficient |
|---|---|---|---|---|---|---|---|
| | Red | Green | Blue | Experimental | Predicted | | |
| M1 | 100 | 0 | 0 | 105.2 | 105.1 | 0.12 | 0.999 |
| M2 | 83.3 | 16.7 | 0 | 109.2 | 109.8 | 0.58 | 0.999 |
| M3 | 75 | 25 | 0 | 95.5 | 95.4 | 0.07 | 0.999 |
| M4 | 66.6 | 33.4 | 0 | 97.8 | 98.4 | 0.61 | 0.999 |
| M5 | 58.3 | 41.7 | 0 | 99.1 | 100.2 | 1.10 | 0.995 |
| M6 | 83.3 | 8.4 | 8.3 | 101.2 | 102.0 | 0.78 | 0.997 |
| M7 | 75 | 16.7 | 8.3 | 99.8 | 99.4 | 0.37 | 0.999 |
| M8 | 66.6 | 8.4 | 25 | 109.7 | 111.0 | 1.18 | 0.997 |

Downloaded from trj.sagepub.com at De Montfort University on September 8, 2011

which are outside of the main body of the yarn and were not accounted for.

The results discussed above allow us to make a conclusion that the probabilities $p_{ij}$, $p_{it}$, and $p_{in}$ found from resolving the minimization problem, expressed by equation 8, properly characterize the migration of fibres between the ring zones and the flow of incoming and terminating fibres which together provide a dynamic equilibrium of the yarn structure. These probabilities will be used for the three-dimensional simulation of melange yarns in the next section. Table 5 presents a typical example of migration probabilities found for yarn sample Y1.

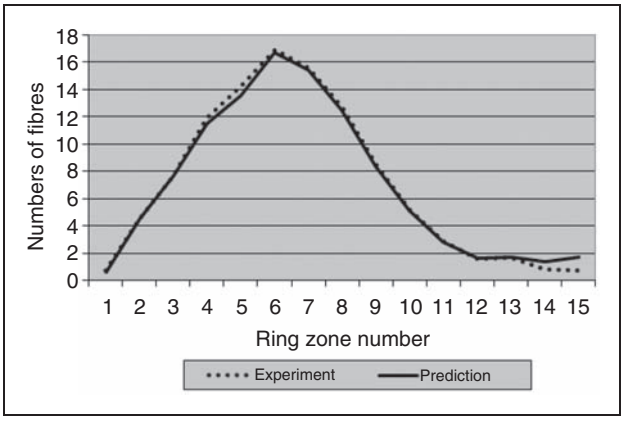



**Figure 7.** Predicted and experimental distribution of the number of fibres in the yarn zones for a melange yarn sample M1.

## *Yarn images generated by the simulation algorithm*

The yarn structure simulation algorithm already presented was implemented in Visual C++ on a PC running a Windows XP operating system. The OpenGL rendering engine version 2.0 was used to produce the three-dimensional images of melange yarn structures. The resulting software system is a MDI (multiple document interface) graphical computer program that can be used to simulate the structures of melange yarns based on various characteristics such as colour composition, linear density, twist level and fibre

**Table 4.** Experimental and predicted average number of fibres for samples series S

| Sample | Yarn linear density, tex[a] | Yarn twist level, tpm[a] | Total number of fibres | | Relative error, % | Correlation coefficient |
|---|---|---|---|---|---|---|
| | | | Experimental | Predicted | | |
| S1 | 55 | 674 | 86.7 | 82.9 | 4.41 | 0.950 |
| S2 | 55 | 337 | 88.7 | 95.1 | 7.23 | 0.996 |
| S3 | 90 | 395 | 177.3 | 179.2 | 1.06 | 0.996 |
| S4 | 55 | 505 | 94.4 | 89.0 | 5.67 | 0.980 |

[a]Yarn linear density and twist level are according to Table 7 in Part I.[1]

**Table 5.** Migration probabilities for yarn sample Y1

| Ring zone | Probability to migrate | | The probability for a new fibre to come into the zone | The probability for a fibre to terminate in the zone |
|---|---|---|---|---|
| | Inwards | Outwards | | |
| 0 | 0 | 0.539 | 0.785 | 0.360 |
| 1 | 0.120 | 0.080 | 0.701 | 0.044 |
| 2 | 0.240 | 0.120 | 0.701 | 0.046 |
| 3 | 0.249 | 0.720 | 0.700 | 0.020 |
| 4 | 0.080 | 0.219 | 0.700 | 0.020 |
| 5 | 0.080 | 0.001 | 0.099 | 0.102 |
| 6 | 0.480 | 0.011 | 0.099 | 0.132 |
| 7 | 0.499 | 0.108 | 0.047 | 0.392 |
| 8 | 0.480 | 0.004 | 0.028 | 0.441 |
| 9 | 0.499 | 0.000001 | 0.020 | 0.496 |
| 10 | 0.499 | 0.000001 | 0.000001 | 0.500 |
| 11 | 0.799 | 0 | 0.036 | 0.200 |

Downloaded from trj.sagepub.com at De Montfort University on September 8, 2011

characteristics. Fibre characteristics include fibre diameter, length and linear density; it is assumed that each of these follows a normal distribution with known average and standard deviation. Fibre characteristics are given in Table 2.

Figure 8a shows the computer generated three-dimensional image of the yarn sample M1 made out of red fibres, the characteristics of which are given in Table 2. The computer generated three-dimensional image of the melange yarn sample M4 which is composed of fibres of two different colours (66.6% red and 33.4% green) is depicted in Figure 8(b). This also shows that the model introduced in this paper can be used to generate three-dimensional images of solid shade yarns as well as melange yarns. Figure 9 presents microscopic images of yarn samples M1 and M4. The comparison between the images shows that the model correctly predicts one of the main visual characteristics of the yarn which is the yarn diameter.

The GUI of the software provides a number of facilities which allow viewing the yarn image from different angles in three-dimensions and obtaining additional information about the yarn; these are as follows:

- Translation, to visualize different parts of the yarn image in order to observe the yarn unevenness;
- Rotation around $x$-, $y$- or $z$-axes to visualize the yarn three-dimensional images from different angles in a three-dimensional space;
- Light position, to simulate the visualization of the yarn image in different lighting conditions;
- Zoom, to visualize the yarn structure at different levels of detail so as to understand better the behaviour of individual fibres within the yarn body, including the formation of yarn hairiness;
- Cross-sections of a simulated yarn can also be taken at any position along the yarn length and visualized, giving a better insight about fibre distribution in ring zones, yarn packing density and yarn hairiness (represented by isolated fibres outside the yarn main body). A computer generated cross-section of the melange yarn samples M1 and M4 are given in Figures 10a and b for illustration; Figure 11 gives examples of the yarn cross-section obtained in the experiment for samples M1 and M4. The comparison between the experimental and computer-generated cross-sections presented in Tables 1, 3, and 4 showed a high level of correlation as discussed previously.
- An average colour of the simulated melange yarn was calculated and compared with the colour characteristics of the real yarn obtained using a spectrophotometer in similar lighting conditions; a detailed discussion on the prediction of the colour of melange yarn will be given in Part III.

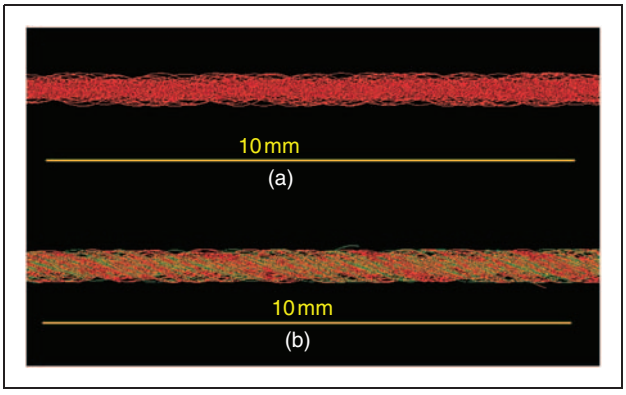



**Figure 8.** Computer generated images of yarns: (a) sample M1, (b) sample M4.

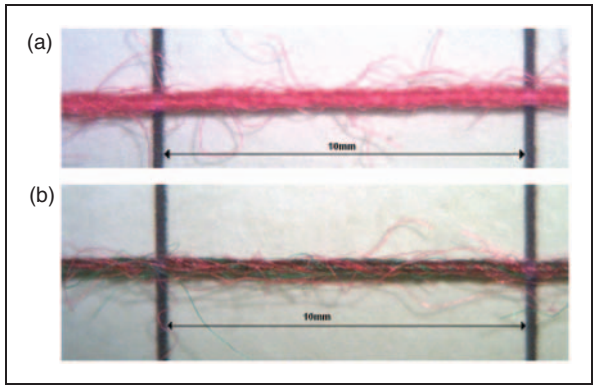



**Figure 9.** Microscopic images of melange yarn samples: (a) sample M1, (b) sample M4.

## Discussion of influencing factors

The three sections that follow discuss different approaches to further improve the proposed methods.

### *Randomization of migration probabilities*

An additional experiment was conducted in order to gather information on the dynamic change in the number of fibres in the consecutive yarn cross-sections. For this, 200 yarn cross-sections were taken at 0.5 mm intervals and processed. Figure 12 shows the number of fibres in the first 100 cross-sections over the first four central zones. It can be seen that the number of fibres in the ring zones never converges to a steady-state value. This can be explained by the action of random factors which affect the local conditions of fibre migration. This effect can be modelled if one assumes that the

Downloaded from trj.sagepub.com at De Montfort University on September 8, 2011

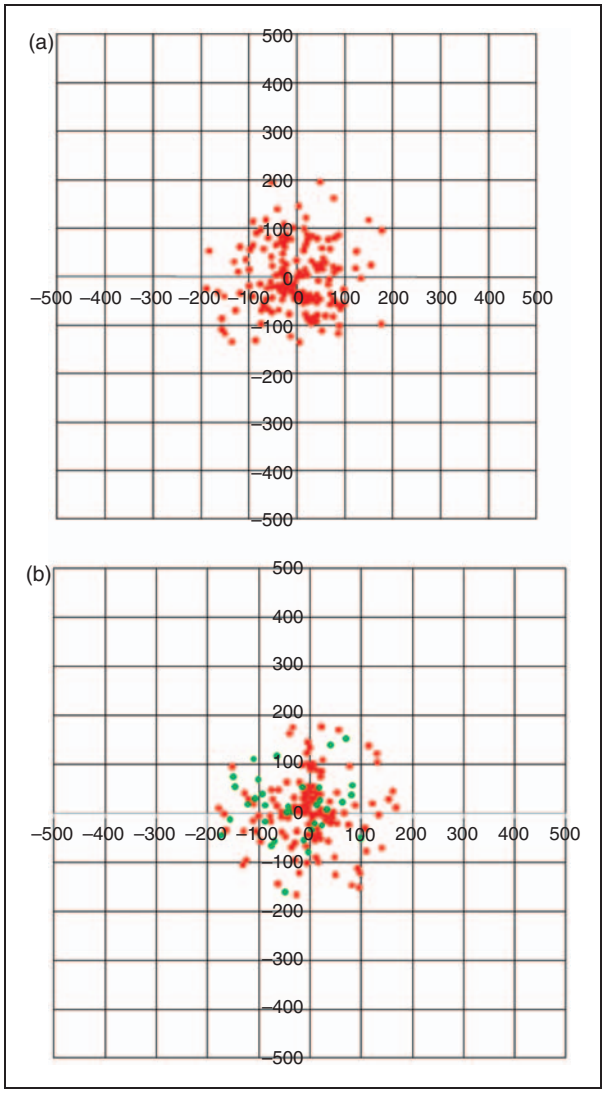



**Figure 10.** Computer-generated images of yarn cross-sections: (a) sample M1, (b) sample M4.

probabilities $p_{ij}$, $p_{it}$, and $p_{in}$ are not fixed but have a different value at each cross-section. As the first approximation, it can be assumed that the above probabilities have a constant component and a random component which depends on the cross-section number as follows:

$$\left.\begin{aligned} p_{ij}^{L} &= p_{ij}^{c} + \xi_{ij}^{L} \\ p_{it}^{L} &= p_{it}^{c} + \xi_{it}^{L} \\ p_{in}^{L} &= p_{in}^{c} + \xi_{in}^{L} \end{aligned}\right\}; \qquad (11)$$

where $p_{ij}^{L}$, $p_{it}^{L}$, and $p_{in}^{L}$ are the probabilities for a fibre to migrate, to terminate, and for a new fibre to arrive at the cross-section $L$, respectively; $p_{ij}^{c}$, $p_{it}^{c}$, and $p_{in}^{c}$ are the constant components of the above probabilities; $\xi_{ij}^{L}$, $\xi_{it}^{L}$, and $\xi_{in}^{L}$ are the uniformly distributed random components of the above probabilities.

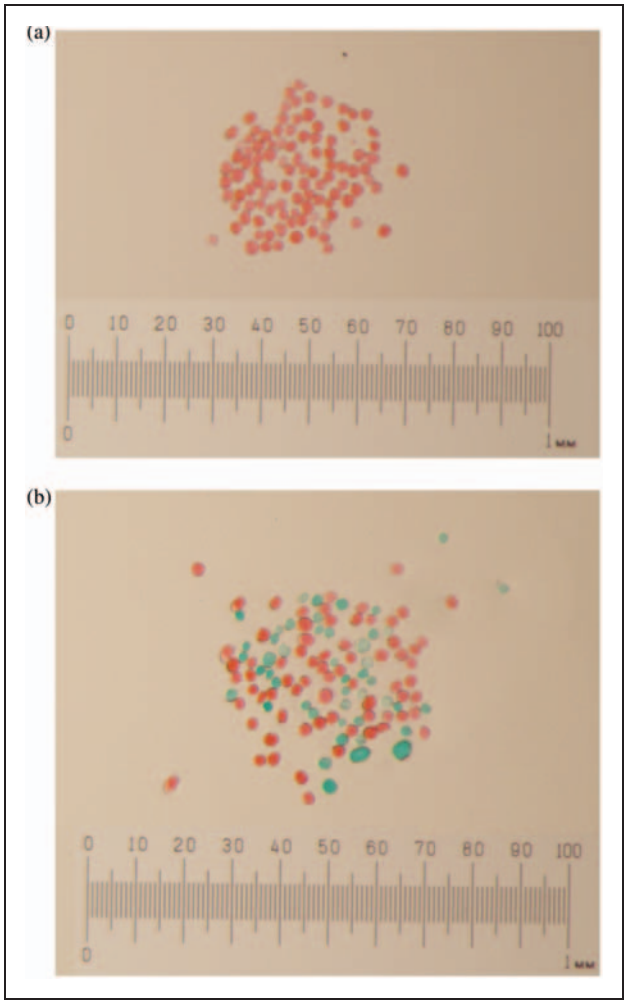



**Figure 11.** Images of the yarn cross-section obtained in the experiment: (a) sample M1, (b) sample M4.

In the general case the probabilities $p_{ij}$, $p_{it}$, and $p_{in}$ can be any appropriate functions of the cross-section position along the yarn axis.

Figure 13 shows an example of yarn simulation where the probabilities $p_{ij}$ and $p_{it}$ were fixed to the same values as for the simulation in Figure 3 but the probability for a new fibre coming into a VL, $p_{in}^{L}$, was calculated according to Equation 11. In this way the flow of new fibres coming into the ring zones was assumed to be an inhomogeneous Poisson process. It can be seen that due to the random change in the value of $p_{in}^{L}$ at each cross-section the number of fibres in the ring zones 0 to 3 never converges to a steady-state condition but fluctuates at the average levels of $\bar{n}_0 = 0.45$, $\bar{n}_1 = 2.25$, $\bar{n}_2 = 4.32$, and $\bar{n}_3 = 4.14$, respectively, with standard deviations of $\sigma_0 = 0.04$, $\sigma_1 = 0.22$, $\sigma_2 = 0.51$, and $\sigma_3 = 0.73$, respectively. This simulation, however, was not an attempt to accurately mimic the migration behaviour of fibres in a real yarn like that presented in Figure 12 but to show the effect caused by

Downloaded from trj.sagepub.com at De Montfort University on September 8, 2011

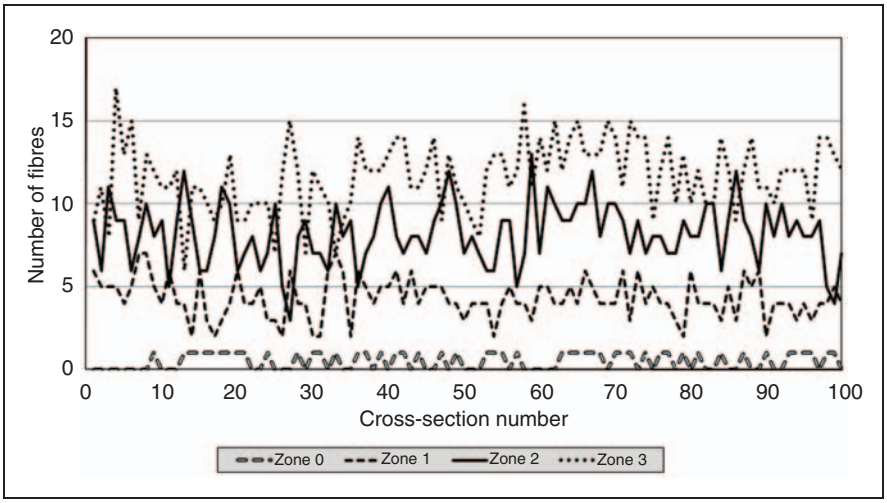



**Figure 12.** Experimental results on the number of fibres in the ring zones.

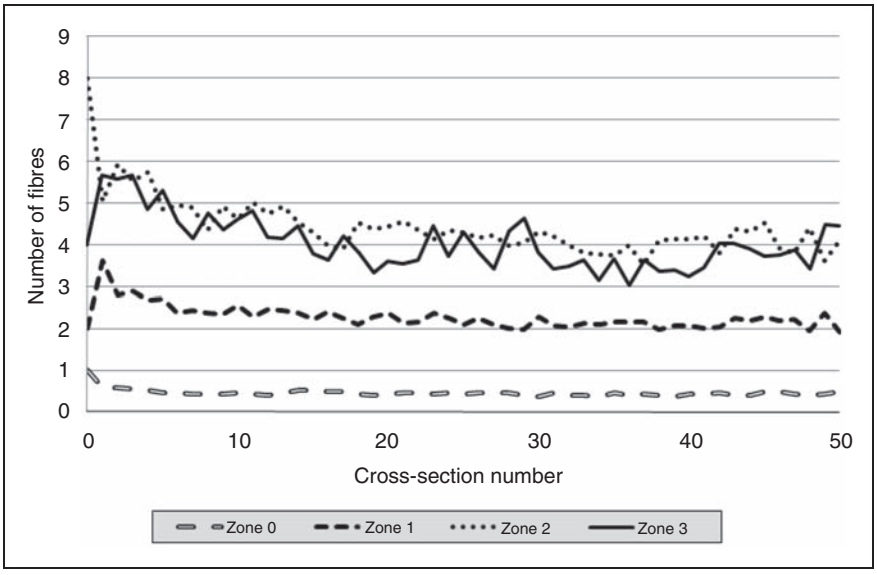



**Figure 13.** Simulated number of fibres in the ring zones using randomized probabilities.

randomization of one of the probabilities. A more accurate model involving all randomized probabilities can be developed on this basis.

## *Potential energy of fibre deformation and fibre migration probabilities*

Fibre migration is a complex process which is governed by two mechanical principles:

- the principle of *minimum energy of deformation*, which says that a fibre is likely to follow a path that minimizes its potential energy of deformation, and
- the principle of *energy conservation*, which states that the total amount of energy of an isolated system remains constant. That is, energy cannot be created or destroyed, although it can be changed from one form to another (e.g. potential energy can be transformed into kinetic energy).

When a fibre is assembled into a yarn with twist, it lies in a helical-like path. In this three-dimensional arrangement, the fibre is subject to tension, bending and twist deformation. Let the three-dimensional curve of a fibre be described in a parametric form by a vector

$$\vec{V}(t) = x(t)\vec{i} + y(t)\vec{j} + z(t)\vec{k}. \qquad (12)$$

Downloaded from trj.sagepub.com at De Montfort University on September 8, 2011

The knowledge of this curve enables the potential energy of elastic deformation associated with the fibre tension, bending, and twisting to be calculated using methods discussed, for example, in Tao[19]and Love.[20] This approach can be applied to the description of fibre migration during yarn formation as well as to the study of yarn structure after it has been spun in which case the energy will be the function of the fibres' varying strains.

In accordance with the principle of minimum potential energy of deformation, the probability that a fibre migrates into a given VL would be greater if the potential energy of deformation of the fibre along its path to that VL is smaller as has been suggested by Grishanov et al.[11] This is illustrated in Figure 14a where $U_i^L$ and $U_i^{L+1}$ are potential energies of fibre $i$ in two consecutive cross-sections $L$ and $L+1$, respectively.

However, a fibre may not migrate into the VL that yields to a minimum potential energy of deformation because there are other fibres competing for the same position or the current level of energy is not high enough to overcome friction between fibre $i$ and surrounding fibres that prevents migration. For the migration to happen this fibre should be at the position corresponding to a higher energy level, Figure 14b. Alternatively, fibre $i$ may be 'assisted' to migrate into a position of lower energy level by a neighbouring fibre $j$ which has a higher level of energy, Figure 14c. There is a probability that the fibre $i$ may be forced to migrate into a VL corresponding to a higher level of energy by the migration of another fibre, $j$, which has a much higher level of energy than fibre $i$; this case is illustrated in Figure 14d.

In a situation where many fibres exhibit the same or similar energies of deformation, only one of them will occupy the VL due to a number of random factors which are difficult to take into account.

It can be seen that the level of energy which a fibre has at the current cross-section, $L$, depends on the fibre path to that cross-section. The migration which may take place between the current and the next cross-section, $L+1$, will be influenced by the previous migrations and thus it is no longer possible to consider the fibre migration as a memoryless process. Figure 15 illustrates possible migrations of a fibre between previous cross-section, $L-1$, and the current cross-section. Path A is for a slack fibre from Group 3 which is approximately parallel to the yarn axis and did not migrate the previous time; this fibre has the lowest level of energy. Paths B and C are for fibres from

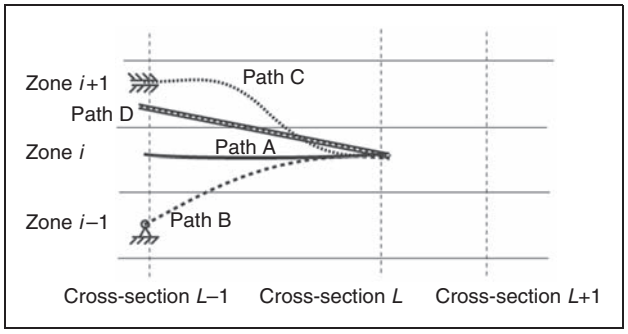



**Figure 15.** Fibre paths to the current cross-section.

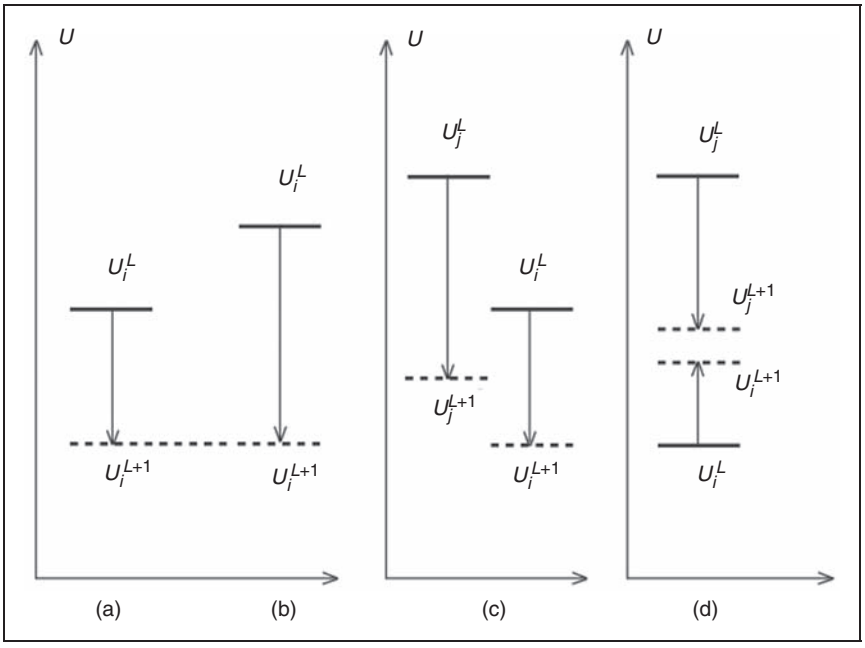



**Figure 14.** Energy levels in migrating fibres.

Downloaded from trj.sagepub.com at De Montfort University on September 8, 2011

Group 1 or Group 2 where Path C shows a higher level of energy than that of B due to the difference in boundary conditions at cross-section $L-1$. The difference is that the fibre on Path B may rotate at cross-section $L-1$ whereas the orientation of Path C is fixed. Path D is for a fibre from Group 3 under tension which has the highest energy level out of these four cases. Whether or not the fibre at cross-section $L$ will migrate between cross-sections $L$ and $L+1$ and in which way depends on the presence or absence of the fibres in the neighbouring VLs, their paths in previous migrations, and their current levels of energy.

Thus it can be said that the fibre migration pattern is affected by both pre-defined conditions related back to the history of previous migrations and random factors defined by local conditions. It should be expected that the influence of the migration pre-history would be limited to a few previous migration events because migration leads to fibre entanglement which restricts freedom of fibre movement. It would not be possible to find a complete analytical solution to the problem of fibre migration due to the large number of factors affecting the process but rather to define conditions which should be used in the migration modelling algorithm. In the framework of this approach it is possible to define migration probabilities as functions of potential energy of fibre deformation.

In accordance with the yarn model proposed in Part I,[1] a fibre in a VL $(i,r)$, $0 \le i < K$ and $0 \le r < [2\pi i]$, can migrate into one of the neighbouring virtual locations $(j, s)$ with probability $p_{ir;js}$ at a steady-state. Recall that a pair $(i, r)$, refers to the virtual location $r$ of the zone $i$ and $K$ is the maximum number of ring zones in the yarn cross-section. We let $I_{ir}$ denote the set of virtual locations $(j, s)$ which are neighbours to the virtual location $(i, r)$ with respect to Definition 3.1 in Part I,[1] including the VL $(i, r)$ itself. We also let $U^L_{ir;js}$ denote the total potential energy of fibre elastic deformation along a fibre path when the fibre, which has either its leading or trailing end free to migrate, migrates from the VL $(i, r)$ in the cross-section $L \ge 0$ into a VL $(j,s) \in I_{ir}$ in the cross-section $L+1$. These cases were illustrated in Figure 1 by the fibres No 1, 2, 10, and 11 of Group 1 and fibres No 4, 7, 9, 12, and 15 of Group 2. It is assumed that these fibres are not subjected to tensile deformation. According to Tao,[19] the potential energy of deformation for a fibre portion between cross-sections $L$ and $L+1$ can be expressed as follows:

$$U^L_{ir;js} = \int_{\varphi_L}^{\varphi_{L+1}} \left[\frac{EI_x}{2}p^2(\varphi) + \frac{EI_y}{2}q^2(\varphi) + \frac{GI_0}{2}w^2(\varphi)\right]\frac{ds}{d\varphi}d\varphi = W^L_{ir;js}, \quad (13)$$

where $\phi_L$ and $\phi_{L+1}$ are the angular positions of the fibre cross-section at the yarn cross-sections $L$ and $L+1$, respectively (see Figure 5); $E$ and $G$ are Young's and shear moduli of the fibre material, respectively; $I_x$, $I_y$ and $I_0$ are moments of inertia of the fibre cross-section with respect to the principal axes and the central axis, respectively; $p$ and $q$ are curvature components of the fibre axis in the principal directions of the fibre cross-section; $w$ is the fibre torsion; $s$ is the curvilinear co-ordinate along the fibre axis.

Note that the value of $U^L_{ir;js}$ depends on the geometry of the fibre, which can be defined using equation (12).

For the fibres from Group 3 the equation for the potential energy should also include a term related to the tensile deformation as follows:

$$U^L_{ir;js} = W^L_{ir;js} + \frac{P_f^2 l}{2EF}, \quad (14)$$

where $P_f$ is the tensile force applied to the fibre; $l$ is the fibre length between the nip of the front rollers and the fibre fixing point in the yarn; $F$ is the area of the fibre cross-section.

It is necessary to take into account the spatial position and the varying number of the fibres in Group 3. In view of this it is convenient to model the cross-section of a multi-layered fibre strand jammed in the nip of the front rollers as a set of virtual locations denoted as $VL_f(u, v)$ where subscript $f$ identifies the fibre strand, $u$ is the layer number, and $v$ is the virtual location number in the layer (Figure 16). Similar to the approach introduced by Grishanov et al.[10] for yarn cross-section, it would be necessary to consider the

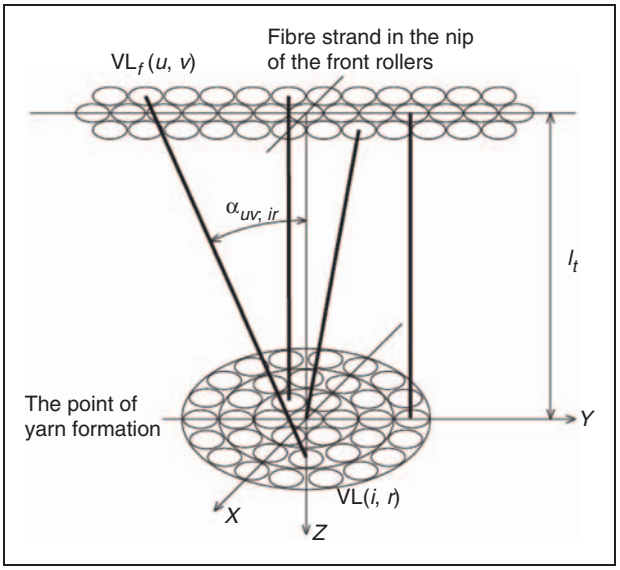



**Figure 16.** Tensioned fibres in the twist triangle.

Downloaded from trj.sagepub.com at De Montfort University on September 8, 2011

fibre distribution in the fibre strand. The angular position of the fibre, $\alpha_{uv;ir}$, with respect to the axis of the yarn being formed, can then be defined through the co-ordinates of $VL_f(u, v)$ in the strand, $VL(i, r)$ in the yarn which this fibre occupies, and the length of twist triangle $l_t$. The angular position of the fibre is subject to a continuous change due to the fibre migration and the rotation of the yarn cross-section in spinning. It is clear that due to the distribution of the fibres in the strand and in the yarn cross-section there might be several fibres which would lie parallel to the yarn axis but not necessarily located in the centre of the yarn cross-section.

Assuming that the flow of newly arriving fibres is a homogeneous Poisson process with a constant rate $\lambda^0_{ir}$, the number of fibres currently present in the twist triangle can be estimated as $l_t\lambda^0_{ir}$. The number of fibres in Group 3 can be assumed to be $n_3 = l_t\lambda^0_{ir}/3$. Let $T_y$ be the yarn tension in spinning such that the fibres that are parallel to the yarn axis are not tensioned. Assuming that fibres under tension are straight, the force applied to each individual fibre, $T_{fi}$, then can be found through the condition that $T_y = \sum_{i=1}^{n_3} T_{fi}\cos\alpha_{uv;ir}$.

The probability that a fibre migrates from a virtual location $(i,r)$ in a cross-section $I$, $0 \le i < K$ and $0 \le r < \lfloor 2\pi i \rfloor$, into one of its neighbours $(j, s) \in I_{ir}$ in the cross-section $L+1$ is defined as follows:

$$p^L_{ir;js} = \frac{\left(\sum_{(m,n)\in I_{ir}} U^L_{ir;mn}\right) - U^L_{ir;js}}{(|I_{ir}| - 1)\sum_{(m,n)\in I_{ir}} U^L_{ir;mn}}. \tag{15}$$

where $I_{ir}$ stands for the number of elements in the set $I_{ir}$.

For any cross-section $L$ of a yarn, this probability distribution satisfies the following requirements, provided that $\sum_{(m,n)\in I_{ir}} U^L_{ir;mn} \ge 0$, for $0 \le i < K$ and $0 \le r < \lfloor 2\pi i \rfloor$ (this condition will be satisfied in the majority of cases because it is very unlikely that the fibres will not have any deformation):

1. The values of $p^L_{ir;js}$ are non-negative, i.e.

$$p^L_{ir;js} \ge 0. \tag{16}$$

for $0 \le i < K$, $0 \le r < \lfloor 2\pi i \rfloor$ and $(j, s) \in I_{ir}$;

2. The normalization requirement is satisfied, i.e.

$$\sum_{(j,s)\in I_{ir}} p^L_{ir;js} = 1, \tag{17}$$

$0 \le i < K$ and $0 \le r < \lfloor 2\pi i \rfloor$;

3. The higher the potential energy of fibre deformation related to the fibre path from one virtual location to another, the lower the probability for the fibre to migrate into that virtual location, i.e.

$$U^L_{ir;js} \ge U^L_{ir;mn} \Rightarrow p^L_{ir;js} \le p^L_{ir;mn}. \tag{18}$$

for $0 \le i < K$, $0 \le r < \lfloor 2\pi i \rfloor$ and $(j, s), (m, n) \in I_{ir}$.

Due to the properties expressed by Equations 16 and 17 the migration probabilities $p^L_{ir;js}$ can be normalized and used in the same way as it has been done in Equation 3.

Figure 17 illustrates the dependence of migration probability on potential energy of deformation where $R_1$, $R_2$, and $R_3$ are radii of curvature associated with the three possible paths of migration between cross-sections $L$ and $L+1$. It can be seen that out of the three paths of fibre migration Path 1, which is an inward migration from zone $i$ to zone $i-1$, presents the lowest energy of deformation whereas Path 3 (an outward migration from zone $i$ to zone $i+1$) corresponds to the highest energy due to the difference in curvature. A more detailed analysis of curvature in migrating fibres shows that the difference in energy can be two orders of magnitude. Thus, the probability of a fibre to migrate along Path 3 will be the lowest according to Equation 15 and the probability to follow Path 1 will be the highest. In this way the probability to migrate is affected by previous migrations, which define the fibre shape up to the point under consideration, and by the continuity of the fibre which in this example act together in favour of preserving the current direction of

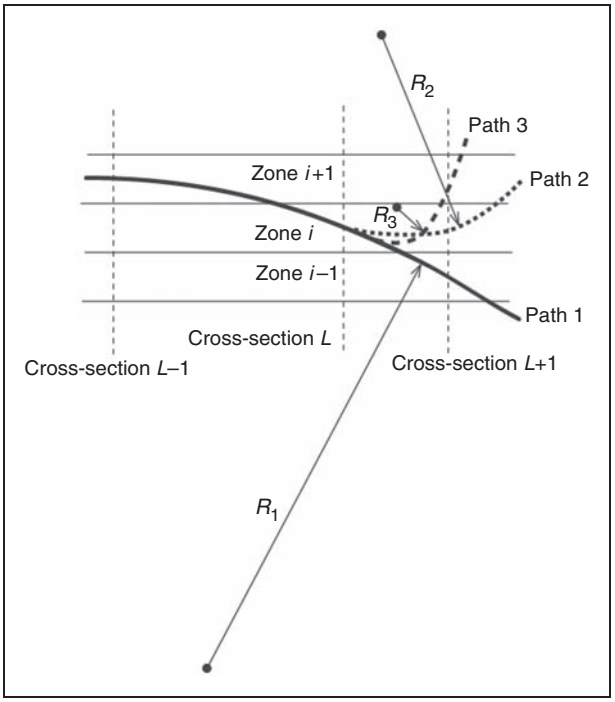



**Figure 17.** Migration paths.

Downloaded from trj.sagepub.com at De Montfort University on September 8, 2011

migration. In a similar manner it is not difficult to imagine a case of no migration which gives the lowest level of energy out of all possible paths.

It is interesting to compare the levels of energy due to the tensile, bending, and twisting deformation. For an acrylic fibre of 23.5 μm in diameter (see Table 2) under tension of $T_f = 4.0\,\mathrm{cN}$ the energy per unit fibre length can be estimated as $U^L_{ir;js} = \frac{T_f^2}{2E_T F} = 3.07 \times 10^{-4}\,\mathrm{J/m}$, where $F$ is the fibre cross-section area and $E_T = 6.0\,\mathrm{kN/mm^2}$ is the tensile Young modulus.[21]

The analysis of three-dimensional fibre migration data obtained in Part I[1] enabled the curvature $\kappa = \frac{1}{\rho_\kappa} = \frac{|V' \times V''|}{|V'|^3}$ and the torsion $\tau = \frac{1}{\rho_\tau} = \frac{|V'V''V'''|}{|V' \times V''|^2}$ of fibres to be estimated, where $V'$, $V''$, and $V'''$ are the first, the second, and the third derivatives of a vector defined by Equation 12 with respect to parameter $t$. This analysis showed that for the same fibre as above, the energy related to bending deformation per unit fibre length can be estimated as being between $U^L_{ir;js} = \frac{E_B I}{2}(\kappa^2 + \tau^2) = 0.60 \times 10^{-4}\,\mathrm{J/m}$ and $52.6 \times 10^{-4}\,\mathrm{J/m}$, where $I$ is the moment of inertia of the fibre cross-section, $E_B = 7.0\,\mathrm{kN/mm^2}$ is Young modulus in bending.[21] The energy related to fibre twisting was estimated to be $0.89 \times 10^{-4}\,\mathrm{J/m}$ for yarn sample S2 (Table 4) and $3.49 \times 10^{-4}\,\mathrm{J/m}$ for sample S1. For a fibre following a perfect helical path in zone 5 and zone 10 the energy associated with bending was found to be $2.25 \times 10^{-4}$ and $1.91 \times 10^{-4}\,\mathrm{J/m}$, respectively.

Comparing these results it can be seen that the model of fibre migration in staple fibre yarns should take into account local conditions of migration defined by fibre twisting, bending and tension.

If a yarn consists of several components which differ in their diameter and/or mechanical properties then the magnitude of energy due to elastic deformation will be different for different components located at neighbouring VLs. It then follows from Equation 15 that the migration probabilities for different components will be different resulting in a preferential outward or inward migration of one of the blend components.

The actual mechanism of fibre migration in spinning inhomogeneous blends deserves special attention, particularly with regard to variation in migration condition caused by mechanical and surface properties such as friction, which is beyond the scope of this paper. This is particularly important in the view of contradictory results reported with regards to preferential migration of fibres with different properties. For example, there is evidence of preferential outward migration of flax fibres in flax/cotton yarns[22,23] whereas Xu et al.[24] presented results on the preferential inward migration of flax fibres. Moreover, an experimental investigation[25] pointed to a different migration behaviour of the same blend in ring spinning and open-end spinning.

## Modelling periodical migration

The periodic pattern of fibre migration can be modelled if one assumes that the three-dimensional co-ordinates, that define the fibre path through the yarn body, are random functions with a known co-variance matrix. Indeed, fibre position in the yarn can be defined by its radial position, $R$, with respect to the yarn axis, its angular position, $\varphi$, and distance along the yarn axis, $z$. The angular co-ordinate $\varphi$ has two components as follows:

$$\varphi(z) = \varphi_1(z) + \varphi_2(z), \tag{19}$$

where $\varphi_1(z)$ is a random component due to angular migration considered in Part I;[1]

$\varphi_2(z) = 2\pi T z$ is linearly increasing with distance $z$ due to twist; $T$ is the yarn twist level.

Component $\varphi_2\,(z)$ defines the new angular position of the whole yarn cross-section and does not affect the numbering of virtual locations within the cross-section (see Figure 5). Subtaction of the linear part from co-ordinate $\varphi\,(z)$ would leave only the random component in which case it can be assumed that $R\,(z)$ and $\varphi_1\,(z)$ are two independent random variables which are random functions of $z$ Let $C_R C_\varphi$ be the co-variance matrices of functions $C_R C_\varphi$ respectively. Modelling the fibre path is then equivalent to the generation of a series of random numbers which collectively represent one realization of the random function. These can be generated as follows:[26,27]

$$R(z_L) = \alpha_L + \sum_{k=1}^{L} \beta_{Lk} x_k; \tag{20}$$

$$\varphi_1(z_L) = \gamma_L + \sum_{k=1}^{L} \delta_{Lk} y_k; \tag{21}$$

where $\alpha_L$and $\gamma_L$ are mean values of $R(z_L)$ and $\varphi_1(z_L)$, respectively; $\beta_{Lk}$ and $\delta_{Lk}$ are coefficients of triangular matrices $B$ and $\Delta$, respectively; $x_k$ and $y_k$ are normally distributed independent random variables with a zero mean and standard deviation of one; $L$ is the current cross-section number.

The coefficients $\beta_{Lk}$ and $\delta_{Lk}$ of triangular matrices $B$ and $\Delta$ can be found as a solution of the equations that follow:

$$BB^{\mathrm{T}} = C_R; \tag{22}$$

$$\Delta\Delta^{\mathrm{T}} = C_\varphi. \tag{23}$$

The values of $R\,(z_L)$ and $\varphi_1\,(z_L)$ generated in this way are normally distributed dependent random variables.

Downloaded from trj.sagepub.com at De Montfort University on September 8, 2011

The co-variance matrices $C_R$ and $C_\varphi$ can be obtained from the correlation analysis of the paths of individual fibres in the yarn using a tracer fibre technique.[3,8,11] Thus this method has an advantage of generating fibre paths with correct statistical properties because it takes into account correlation between fibre positions in previous migrations and at the same time the migration process is not considered as memoryless.

As soon as the co-ordinates $R(z_L)$ and $\varphi_1$ $z_L$) are known\comma the virtual locations for the fibre path can be found as follows:

$$r = \left\lfloor \frac{R(z_L)}{d} + 0.5 \right\rfloor; \quad (24)$$

$$r = \left\lfloor \frac{\varphi_1(z_L)\lfloor 2\pi i \rfloor}{2\pi} + 0.5 \right\rfloor; \quad (25)$$

where $d$ is the ring zone width; $T$ is the yarn twist level; $i$ and $r$ are the zone number and the VL number, respectively.

The approaches discussed in this section will be further investigated and implemented in more advanced versions of the yarn structure simulation algorithm described above.

## Conclusion

A queuing model was used in Part I[1] of this series to describe the migration behaviour of fibres in a yarn. In Part II, a new method for estimating the migration probabilities and the distribution of the number of fibres in the ring zones was suggested. The correlations between predicted and experimental real yarn examinations were excellent. On the basis of this a yarn structure simulation algorithm was developed which used the migration probabilities method to predict the distribution and migration patterns of fibres in melange yarns. It was shown that this algorithm can be used to accurately simulate three-dimensional images of melange yarns from technical specification. Due to the generic nature of the model and the algorithm it is possible to apply this method for the simulation of a wide range of yarns including ring-spun and open-end spun yarns which can be of solid shade or produced from melange blends. Currently, testing has only been carried out on three colour melange yarns but future work will introduce a higher range of coloured fibre components.

The analysis of energy associated with deformation of migrating fibre showed that fibre migration is affected by previous migrations and boundary conditions together with local conditions defined by fibre tension, bending, and twisting.

In addition, future work will also examine the role of the memoryless assumption inherent to *homogeneous Poisson processes* underpinning the yarn model. Rather *inhomogeneous Poisson processes*, as defined by the dynamic form of *Palm's theorem*,[28] will be considered. In such a model, the fibre migration process is not memoryless but a function of the history of previous fibre migrations.

## Funding

This work was supported by the EPSRC (grant numbers GR/S77325/01 and GR/S77318/01).

## References

1. Siewe F, Grishanov S, Cassidy T and Banyard G. An application of queuing theory to modelling of melange yarns. Part I: A queuing model of melange yarn structure. *Textile Res J* 2009; 79(16): 1467–1485.
2. Hearle JWS and Merchant VB. Interchange of position among the components of a seven-ply structure: mechanism of migration. *J Textile Inst* 1962; 53: T537–T552.
3. Hearle JWS, Gupta BS and Merchant VB Migration of fibres in yarns. Part I: Characterization an idealization of migration behaviour. *Textile Res J* 1965; 35: 329–334.
4. Hearle JWS, Gupta BS and Goswami BC. The migration of fibres in yarns: Part V: the combination of mechanisms of migration. *Textile Res J* 1965; 35: 972–978.
5. Hearle JWS and Bose ON. The form of yarn twisting. Part I: Ideal cylindrical and ribbon-twisted forms. *J Textile Inst* 1966; 57: T294 – T307.
6. Hearle JWS and Bose ON. The form of yarn twisting. Part II: Experimental studies. *J Textile Inst* 1966; 57: T308–T320.
7. Hearle JWS and Goswami BC. Migration of fibers in yarns. Part VIII: Experimental study on a 3-layer structure of 19 filaments. *Textile Res J* 1970; 40: 598–607.
8. Riding G. Filament migration in single yarns. *J Textile Inst* 1964; 55: T9–T17.
9. Treloar LRG. A migrating-filament theory of yarn properties. *J Textile Inst* 1965; 56: T359–T380.
10. Grishanov SA, Lomov SV, Cassidy T and Harwood RJ. The simulation of the geometry of two component yarns. Part II: Fibre distribution in the yarn cross section. *J Textile Inst* 1997; 88: 352–372.
11. Grishanov SA, Harwood RJ and Bradshaw MS. A model of fibre migration in staple fibre yarn. *J Textile Inst* 1999; 90: 298–321.
12. Sriprateep K and Bohez ELJ. A new computer geometric modelling approach of yarn structures for the conventional ring spinning process. *J Textile Inst* 2009; 100(3): 223–236.
13. Korn GA and Korn TM. *Mathematical handbook for scientists and engineers*. New York: McGraw-Hill, 1968, p.1130.
14. Hickie TS and Chaikin M. Some aspects of worsted-yarn structure. Part III: The fibre-packing density in the cross-section of some worsted yarns. *J Textile Inst* 1973; 65: 433–437.

Downloaded from trj.sagepub.com at De Montfort University on September 8, 2011

15. Nechar B, Ishtiaque SM and Svehlova L. Rotor yarn structure by cross-sectional microtomy. *Textile Res J* 1988; 58: 625–632.
16. Jiang XY, Hu JL, Cheng KPS and Postle R. Determining the cross-sectional packing density of rotor spun yarns. *Textile Res J* 2004; 75(3): 233–239.
17. Yilmaz D, Goktepe F, Goktepe O and Kremenakova D. Packing density in compact yarns. *Textile Res J* 2007; 77(9): 661–667.
18. Himmelblau DM. *Applied nonlinear programming*. London: McGraw-Hill, 1972, p.498.
19. Tao X. Mechanical properties of a migrating fibre. *Textile Res J* 1996; 66(12): 754–762.
20. Love AEH. *A triatise on the mathematical theory of elasticity*, 4th ed. New York: Dover Publications, 1944.
21. Morton WE and Hearle JWS. *Physical properties of textile fibres*, 3rd ed. Manchester: The Textile Institute, 1997.
22. Truevtsev NN, Legesina GI, Grishanov SA and Asnis LM. Structural features of flax blended yarns. *Textile Industry* 1995; 6: 21–22.
23. Bogdan AF. An investigation of the technology of flax-containing yarn production. PhD Thesis, De Montfort University, 2008.
24. Xu B and Ma J. Radial distribution of fibres in compact-spun flax-cotton blended yarns. *Fibres and Textiles in Eastern Europe* 2010; 18(1): 24–27.
25. Qu L, Zhang J, Han G, Wang X, Yu A and Zhang B. Comparing the structure of rabbit hair/cotton blended rotor-spun and ring-spun yarns. *Res J Textiles Apparel* 2004; 8(1): 33–37.
26. Knuth DE. The art of computer programming. Vol. 2 Seminumerical algorithms. Reading, MA: Alison-Wesley, 1998.
27. Grishanov S. Fundamental modelling of textile fibrous structures. In: Chen X (ed.) *Modelling and Predicting Textile Behaviour*. Cambridge: Woodhead Publishing, 2009.
28. Grawford GB. Palm's Theorem for non-stationary processes. The Rand Corporation, No R-2750-RC, 1981.
29. Ahlberg JH, Nilson EN and Walsh JL. *The theory of splines and their applications*. New York: Academic Press, 1967.

## Appendix

## Cubic spline approximation of fibre paths

The concept of potential energy of fibre deformation defined in the previous section depends on the underlying geometry of the fibre path. In this section, the geometry of a fibre path is approximated by a three-dimensional cubic spline. The cubic spline[29] is a mathematical function which follows a shape that minimizes its potential energy. The *beam theory*[29] states that this energy is proportional to the integral with respect to the arc length of the square of the curvature of the spline. A cubic spline has first and second derivatives which are continuous. As such, it is smooth and does not break. In this respect, it is reasonable to approximate a fibre path as a three-dimensional cubic spline. Suppose the three-dimensional Cartesian coordinates $(x_i, y_i, z_i)$ of a fibre are known at consecutive cross-sections $i=0, 1,\ldots, n-1$ of a yarn such that the fibre starts at the cross-section 0 and ends at the cross-section $n-1$. The fibre path in each subinterval $[zi, zi+1]$ is approximated by the following three-dimensional curve:

$$\begin{cases} x(t) = R(t)\cos[2\pi\omega(t - z_i) + \theta_i] \\ y(t) = R(t)\sin[2\pi\omega(t - z_i) + \theta_i] \\ z(t) = t \end{cases} \quad \text{(A1)}$$

where $\omega$ is the twist level of the yarn, $\theta_i$ is the angular position of the fibre in the cross-section $i$ and $R(t)$ is a cubic spline defined by

$$\mathrm{R(t)} = \mathrm{d_i(t - z_i)^3 + c_i(t - z_i)^2 + b_i(t - z_i) + a_i} \quad \text{(A2)}$$

for $t\in[zi, zi + 1]$, and $a_i$, $b_i$, $c_i$ and $d_i$ are the spline coefficients in the subinterval $[zi, zi + 1]$.

The function $R$ defined by equation A2 approximates the radial position of the fibre along the yarn axis. The coefficients of the spline are calculated by solving the system of linear equations:

$$\left.\begin{array}{l} R(z_i) = \sqrt{x_i^2 + y_i^2}, 0 \le i \le n-1; \\ \lim\limits_{t\to z_i^-} R(t) = \lim\limits_{t\to z_i^+} R(t), 0 < i < n-1; \\ \lim\limits_{t\to z_i^-} R'(t) = \lim\limits_{t\to z_i^+} R'(t), 0 < i < n-1; \\ \lim\limits_{t\to z_i^-} R''(t) = \lim\limits_{t\to z_i^+} R''(t), 0 < i < n-1; \\ R''(t_0) = 0; \\ R''(t_{n-1}) = 0 \end{array}\right\} \quad \text{(A3)}$$

The A3 equations define the so called natural cubic spline which ensures that as the curve passes through all the known points it is smooth and does not break; it also ensures that the second derivative $R''$ is continuous and that the potential energy of the curve, which is proportional to $\int_{z_0}^{z_{n-1}} [R''(t)]^2 dt$, is minimum.[29]

Downloaded from trj.sagepub.com at De Montfort University on September 8, 2011